Dalton Transactions

Dynamic Article Links

Cite this: *Dalton Trans.*, 2011, **40**, 4590

www.rsc.org/dalton

PAPER

High-spin Ni(II) clusters: triangles and planar tetranuclear complexes†

Athanassios D. Katsenis,[a] Vadim G. Kessler[b] and Giannis S. Papaefstathiou*[a]

Received 5th December 2010, Accepted 23rd February 2011
DOI: 10.1039/c0dt01705a

The exploration of the $NiX_2/py_2CO/Et_3N$ (X = F, Cl, Br, I; py_2CO = di-2-pyridyl ketone; Et_3N = triethylamine) reaction system led to the tetranuclear $[Ni_4Cl_2\{py_2C(OH)O\}_2\{py_2C(OMe)O\}_2(MeOH)_2]Cl_2\cdot 2Et_2O$ (**1**·2Et$_2$O) and $[Ni_4Br_2\{py_2C(OH)O\}_2\{py_2C(OMe)O\}_2(MeOH)_2]Br_2\cdot 2Et_2O$ (**2**·2Et$_2$O) and the trinuclear $[Ni_3\{py_2C(OMe)O\}_4]I_2\cdot 2.5MeOH$ (**3**·2.6MeOH), $[Ni_3\{py_2C(OMe)O\}_4](NO_3)_{0.65}I_{1.35}\cdot 2MeOH$ (**4**·2MeOH) and $[Ni_3\{py_2C(OMe)O\}_4](SiF_6)_{0.8}F_{0.4}\cdot 3.5MeOH$ (**5**·3.5MeOH) aggregates. The presence of the intermediate size Cl^- and Br^- anions resulted in planar tetranuclear complexes with a dense hexagonal packing of cations and donor atoms (tetramolybdate topology) where the X^- anions participate in the core acting as bridging ligands. The F^- and I^- anions do not favour the above arrangement resulting in triangular complexes with an isosceles topology. The magnetic properties of **1–3** have been studied by variable-temperature dc, variable-temperature and variable-field ac magnetic susceptibility techniques and magnetization measurements. All complexes are high-spin with ground states S = 4 for **1** and **2** and S = 3 for **3**.

Introduction

Polynuclear metal complexes based on paramagnetic metal ions continue to attract attention due to their fascinating magnetic properties.[1] Among the numerous metal clusters known today, those which can be isolated in families emerge because they provide the opportunity to draw structure-property relations.[2] Over the last years, polynuclear metal complexes have also emerged as building blocks for the construction of polymeric complexes known as Metal–Organic Frameworks (MOFs).[3] Although only a handful of pre-isolated clusters have been utilized as building blocks for the construction of such materials,[4] there have been developed some exceptional synthetic strategies which lead to cluster-based MOFs where the clusters present in the frameworks have been isolated in the past.[3,5]

Our attention has recently turned toward the exploitation of magnetically interesting metal clusters as building blocks for the construction of supramolecular architectures.[6,7] To this end, we exploited members of a family of trinuclear Mn^{III} complexes[6] of general formulae $[Mn^{III}_3O(R\text{-}sao)_3(X)(L)_3]$ ($saoH_2$ = salicylaldoxime; R = H, Me, Et etc; X = RCO_2^-, ClO_4^-; L = solvent) as building blocks for constructing discrete and infinite supramolecular architectures by means of host–guest interactions and coordination driven self-assembly.

Besides the salicylaldoximato Mn^{III} complexes, we are also exploring the chemistry of di-2-pyridyl ketone (py_2CO, Scheme 1) as a source of polynuclear metal complexes.[8] The rich coordination chemistry of py_2CO originates from its ability to undergo metal assisted nucleophilic attack on the carbonyl carbon atom by small molecules such as H_2O and alcohols (ROH) resulting in the hydrate [$py_2C(OH)_2$, Scheme 1] and hemiacetal [$py_2C(OR)(OH)$, Scheme 1] of py_2CO, respectively. That, in turn, enables py_2CO to act as a polynucleating ligand and has resulted in numerous polynuclear metal complexes.

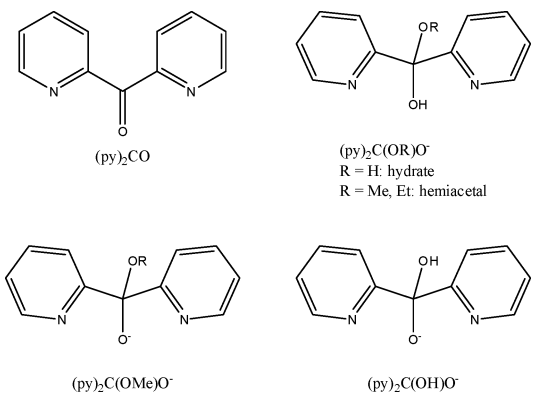

Scheme 1 Ligands discussed in the text.

By exploring the py_2CO/Co^{II} chemistry we demonstrated that the reactivity of the tetranuclear cubane cluster $[Co_4\{(py)_2C(OH)O\}_4(NO_3)_3(H_2O)]NO_3$, $[(py)_2C(OH)O^-$ is

[a]*Laboratory of Inorganic Chemistry, Department of Chemistry, National and Kapodistrian University of Athens, Panepistimiopolis, 157 71, Zografou, Greece. E-mail: gspapaef@chem.uoa.gr; Fax: +30 210-727-4782; Tel: +30 210-727-4840*

[b]*Department of Chemistry, Swedish University of Agricultural Sciences, Box 7015, 750 07, Uppsala, Sweden*

† Electronic supplementary information (ESI) available: Additional Figures and Tables. CCDC reference numbers 803774–803778. For ESI and crystallographic data in CIF or other electronic format see DOI: 10.1039/c0dt01705a

the monoanion of the hydrate of $(py)_2CO$], with 4,4′-bipyridine (4,4′-bpy), resulted in the tetranuclear assembly $[Co_4\{(py)_2C(OMe)O\}_4(4,4'bpy)_2(MeOH)_4](NO_3)_4$, with the latter being regarded as a dimer of dimers.[7] The transformation of the cube to the dimer of dimers has meant that the utilization of pre-isolated clusters as building blocks may result in discrete assemblies instead of polymeric complexes, depending on the stability of the cluster under the reaction conditions.

Following those results, we moved toward the Ni^{II}/py_2CO chemistry. The py_2CO/nickel halide chemistry (NiX_2, X = F, Cl, Br and I) resulted in two planar tetranuclear and three trinuclear aggregates with the tetranuclear clusters to adopt the known defect double cubane topology while the trinuclear complexes adopt a triangular isosceles topology which is new in the py_2CO chemistry. The synthetic aspects as well as the structural and magnetic characterization are discussed.

Results and discussion

Syntheses

Following our previous work on Co(II)/py_2CO chemistry,[7] our initial goal was to synthesize a tetranuclear Ni^{II} cubane cluster in order to use it as a starting material for constructing extended frameworks. The reaction of $NiCl_2{\cdot}6H_2O$ with py_2CO in MeOH followed by the addition of Et_3N resulted in a green solution from which green plate crystals of $[Ni_4Cl_2\{py_2C(OH)O\}_2\{py_2C(OMe)O\}_2(MeOH)_2]Cl_2{\cdot}2Et_2O$ (**1**·2Et_2O) were isolated after Et_2O diffusion. The single-crystal X-ray analysis revealed that the planar tetranuclear assembly had adopted the defect double cubane topology with a $[NiCl_2O_4]^{2+}$ core where two μ_2-Cl^- anions bridge Ni^{II} centres at opposite sites of the core. That, in turn, prompted us to further explore the py_2CO/NiX_2 (X = F, Cl, Br and I) chemistry with the aim of synthesizing a series of defect double cubanes with the $[Ni_4{\times}_2O_4]^{2+}$ core and study the influence of the halide in their magnetic properties. The next member of this family $[Ni_4Br_2\{py_2C(OH)O\}_2\{py_2C(OMe)O\}_2(MeOH)_2]Br_2{\cdot}2Et_2O$ (**2**·2Et_2O) was easily isolated from the reaction of $NiBr_2{\cdot}6H_2O$ with py_2CO in MeOH in the presence of Et_3N following Et_2O diffusion into the reaction mixture. Trying to obtain the iodide analogue by reacting $NiI_2{\cdot}6H_2O$ with py_2CO under the exact same reaction conditions as above we isolated the trinuclear cluster $[Ni_3\{py_2C(OMe)O\}_4]I_2{\cdot}2MeOH$ (**3**·2.6MeOH). Changing the reaction conditions as well as the metal to ligand ratios or even the nature of the base ($LiOH{\cdot}H_2O$, MeONa) did not influence the identity of the product. We then moved toward changing the nature of the starting material and utilized $Ni(NO_3)_2{\cdot}6H_2O$ followed by the addition of an excess of either KI or NaI in MeOH in the presence of Et_3N. The result of these reactions was the trinuclear complex $[Ni_3\{py_2C(OMe)O\}_4](NO_3)_{0.65}I_{1.35}{\cdot}2MeOH$ (**4**·2MeOH) where the initial triangular core was maintained. Knowing the presence of this trinuclear unit in the Ni^{II}/py_2CO chemistry, we attempted to synthesize it by reacting $Ni(NO_3)_2{\cdot}6H_2O$ with an excess of py_2CO in the presence of NaCl or NaBr. The results of these reactions were complexes having identical IR spectra with **1** and **2** (with an exception of a band at ~1380 which is attributed to the presence of NO_3^- anions), suggesting that similar complexes had been obtained. The exploration of the $NiF_2/py_2CO/Et_3N$ reaction system yielded green crystals of $[Ni_3\{py_2C(OMe)O\}_4](SiF_6)_{0.8}F_{0.4}{\cdot}3.5MeOH$ (**5**·3.5MeOH) after a period of a month. The trinuclear core of complex **5** is similar but not exactly the same with the trinuclear core of **4**. The long period for the isolation of this cluster is associated with the extraction of Si (for the SiF_6^{2-}) from the borosilicate glass tube used for crystallizing out the compound.

Description of structures

Complex **1** crystallizes in the monoclinic space group $P2_1/c$ (Table 1). Selected distances and angles are listed in Table S1.† A partially labelled plot of the tetranuclear cation

Table 1 Crystallographic data for complexes **1–5**

Compound reference	**1**	**2**	**3**	**4**	**5**
Chemical formula	$C_{56}H_{68}Cl_4N_8Ni_4O_{12}$	$C_{56}H_{68}Br_4N_8Ni_4O_{12}$	$C_{50\cdot50}H_{51\cdot75}I_2N_8Ni_3O_{10\cdot50}$	$C_{50}H_{50\cdot50}I_{1\cdot50}N_{8\cdot50}Ni_3O_{11\cdot50}$	$C_{101}H_{108}F_{10\cdot40}N_{16}Ni_6O_{21}Si_{1\cdot60}$
Formula mMass	1421.82	1599.66	1368.68	1320.97	2476.84
Crystal system	Monoclinic	Monoclinic	Monoclinic	Monoclinic	Orthorhombic
Space group	*P*21/*c*	*P*21/*c*	*P*21/*c*	*P*21/*c*	*Pbcn*
a/Å	14.098(4)	13.6786(3)	24.004(2)	24.0128(12)	23.105(5)
b/Å	17.364(5)	17.2699(4)	15.6042(14)	15.6980(7)	22.054(5)
c/Å	11.925(4)	11.9272(2)	15.6950(15)	15.7309(7)	23.008(6)
α (°)	90.00	90.00	90.00	90.00	90.00
β (°)	100.253(5)	100.519(2)	99.9160(10)	101.010(2)	90.00
γ (°)	90.00	90.00	90.00	90.00	90.00
V/Å^3	2872.5(14)	2770.19(10)	5790.9(9)	5820.7(5)	11723(5)
Z	2	2	4	4	4
Radiation type	Mo-Kα	Mo-Kα	Mo-Kα	Mo-Kα	Mo-Kα
Reflections measured	17328	34362	34516	33783	90131
Independent reflections	6827	5408	11340	9334	11494
R_{int}	0.0424	0.0419	0.0292	0.0325	0.0647
R_1 ($I > 2\sigma(I)$)[a,b]	0.0462	0.0488	0.0565	0.0778	0.0532
$wR(F^2)$ ($I > 2\sigma(I)$)[c]	0.1195	0.1302	0.1700	0.2088	0.1612
R_1 (all data)[a]	0.0897	0.0603	0.0756	0.0991	0.0748
$wR(F^2)$ (all data)[c]	0.1336	0.1338	0.1804	0.2183	0.1713
GOF on F^2	1.049	1.050	1.078	1.077	1.068

[a] For observed data. [b] $R1 = \Sigma \| F_o | - | F_c \| / \Sigma | F_o |$. [c] $wR2 = [\Sigma w(|F_o^2| - |F_c^2|)^2 / \Sigma w |F_o^2|^2]^{1/2}$.

$[Ni_4Cl_2\{py_2C(OH)O\}_2\{py_2C(OMe)O\}_2]^{2+}$ is shown in Fig. 1. The structure consists of centrosymmetric tetranuclear molecules. The cluster has a $[Ni_4(\mu_2\text{-}Cl)_2(\mu_2\text{-}OR)_2(\mu_3\text{-}OR)_2]^{2+}$ core (Fig. 2) with the four Ni^{II} atoms being coplanar. This core is frequently referred as defective double cubane (two cubanes sharing one face and each missing one vertex). The Ni^{II} atoms bridged by means of two μ_2-Cl^- anions, two μ_2-O atoms from the $(py)_2C(OMe)O^-$ and two μ_3-O atoms from the $(py)_2C(OH)O^-$ ligands (Scheme 2). Peripheral ligation to the distorted octahedral Ni^{II} atoms is provided by

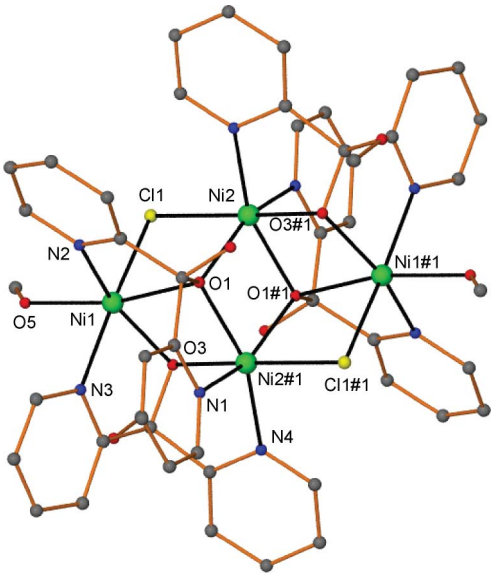

Fig. 1 The molecular structure of complex **1**. All hydrogen atoms have been omitted for clarity. Symmetry code: #1 2–x, 2–y, 1–z.

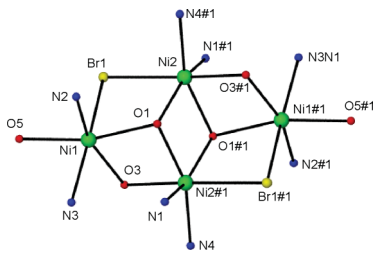

Fig. 2 The $[Ni_4(\mu_2\text{-}Br)_2(\mu_2\text{-}OR)_2(\mu_3\text{-}OR)_2]^{2+}$ core of complex **2**. Symmetry code: #1 –x,1–y,1–z.

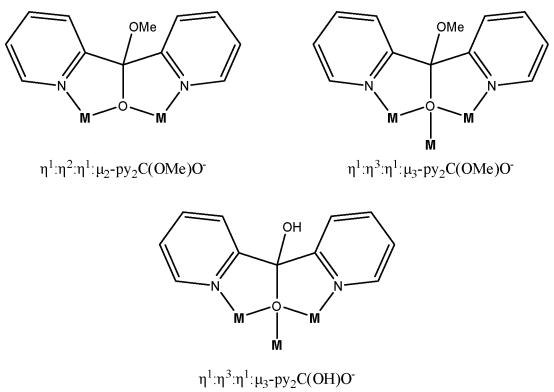

Scheme 2 The coordination modes of $(py)_2C(OMe)O^-$ and $(py)_2C(OH)O^-$.

two O atoms of the terminal MeOH ligands and the N atoms of the eight 2-pyridyl rings. Atoms O1 of two $(py)_2C(OH)O^-$ ligands are triply bridging with distances to Ni^{II} atoms of 2.165(2), 2.028(2) and 2.106(2) Å for Ni1–O1, Ni2–O1#1 and Ni2–O1, respectively. The Ni1–O1–Ni2, Ni1–O1–Ni2#1 and Ni2–O1–Ni2#1 (#1: 2–x,2–y,1–z) angles are 104.37(10), 95.36(9) and 99.33(9)°, respectively. Atoms O3 of the two other $(py)_2C(OMe)O^-$ ligands are doubly bridging with distances of 2.019(2) and 2.126(2) Å to Ni1 and Ni2, respectively. The Ni1–O3–Ni2#1 angle is 96.82(10)°. One O atom of each $(py)_2C(OH)O^-$ ligand remains protonated and unbound to the metals. Therefore, the two $(py)_2C(OH)O^-$ ions adopt the $\eta^1:\eta^3:\eta^1:\mu_3$ coordination mode and the other two $(py)_2C(OMe)O^-$ bind with the $\eta^1:\eta^2:\eta^1:\mu_2$ mode (Fig. 1, Scheme 2). Ni1 and Ni2 are also bridged by one μ_2-Cl^- ligand (Cl1). The Ni–Cl1 and Ni2–Cl1 distances are 2.405(1) and 2.428(1) Å, respectively. The Ni1–Cl1–Ni2 angle is 88.55(4)°. The Ni···Ni distances are 3.374, 3.101, 5.663 and 3.151 Å for the Ni1···Ni2, Ni1···Ni2#1, Ni1···Ni1#1 and Ni2···Ni2#1, respectively.

Complex **2** also crystallizes in the monoclinic space group $P2_1/c$ (Table 1) and is isostructural to complex **1**. The values of most of the bond distances and angles (Table S2†) within the $[Ni_4Br_2\{py_2C(OH)O\}_2\{py_2C(OMe)O\}_2]^{2+}$ (Fig. 2) are very close to those measured in complex **1** with an exception of the Ni–Br distances and Ni–Br–Ni angles. Specifically, the Ni1–O1, Ni2–O1#1 and Ni2–O1 bond distances are 2.168(3), 2.035(3) and 2.104(3) Å, respectively, while the Ni1–O1–Ni2, Ni1–O1–Ni2#1 and Ni2–O1–Ni2#1 angles are 106.19(14), 94.76(13) and 99.60(14)°, respectively (#1: –x,1–y,1–z). The Ni–Br1 and Ni2–Br1 distances are 2.531(1) and 2.564(1) Å, respectively, while the Ni1–Br1–Ni2 angle is 84.19(2)°. The Ni···Ni distances are 3.416, 3.094, 5.700 and 3.161 Å for the Ni1···Ni2, Ni1···Ni2#1, Ni1···Ni1#1 and Ni2···Ni2#1, respectively and compare well with those in complex **1**. The most profound structural change in the $[Ni_4(\mu_2\text{-}Br)_2(\mu_2\text{-}OR)_2(\mu_3\text{-}OR)_2]^{2+}$ core, as compared with the one in complex **1**, is the increase of the Ni1–O1–Ni2 angle from 104.37(10)° (in **1**) to 106.19(14)° (in **2**) which is accompanied with the decrease of the Ni1–X1–Ni2 [X = Cl 88.55(4)° and X = Br 84.19(2)°] angle. The bigger size of the Br^-, as compared with the Cl^-, forces the Ni1 and Ni2 to move apart from each other at about 0.04 Å resulting in the increase of the Ni1–O1–Ni2 angle of about 1.8°.

Complex **3** crystallizes in the monoclinic space group $P2_1/c$ (Table 1). Selected distances and angles are listed in Table S3. Three Ni^{II} ions and four $(py)_2C(OMe)O^-$ anions have assembled to create a cationic trinuclear cluster comprising the $[Ni_3(\mu_2\text{-}OR)_2(\mu_3\text{-}OR)_2]^{2+}$ with the three Ni^{II} ions being arranged at the corners of an isosceles triangle (Fig. 3). All three Ni^{II} atoms are in a distorted octahedral environment with the N atoms of the eight 2-pyridyl rings providing peripheral ligation. Two of the four $(py)_2C(OMe)O^-$ ligands adopt the $\eta^1:\eta^3:\eta^1:\mu_3$ coordination mode and the other two bind with the $\eta^1:\eta^2:\eta^1:\mu_2$ mode (Scheme 2). The Ni–O distances are in the range of 1.938(3) to 2.413(3). Two of the Ni–O distances which involve the triply bridging μ_3-O atoms [Ni2–O3 2.413(3) Å] and [Ni2–O5 2.328(3) Å] are distinguishably longer than the others. The Ni···Ni distances are 2.811, 2.815 and 3.187 Å for the Ni1···Ni2, Ni2···Ni3 and Ni3···Ni1, respectively. The $[Ni_3(O\text{–}R)_4]^{2+}$ core found in **3** is quite rare in Ni^{II} chemistry[9–12] and completely new in the py_2CO chemistry of any metal ion.

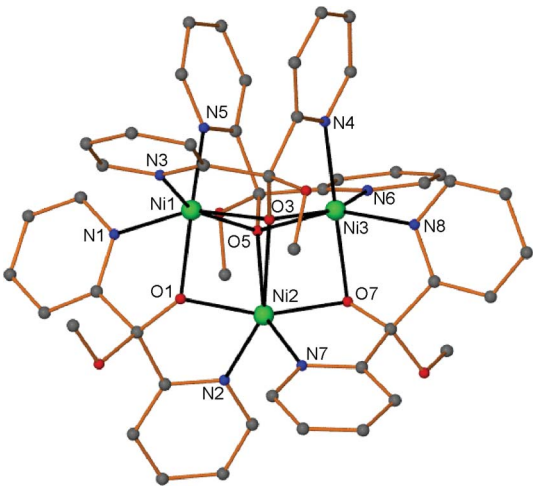

Fig. 3 The molecular structure of complex **3**. All hydrogen atoms have been omitted for clarity.

Complex **4** crystallizes in the monoclinic space group $P2_1/c$ (Table 1, Fig. S1†) and is isostructural to complex **3**. Selected distances and angles are listed in Table S4.† The $[Ni_3(\mu_2\text{-}OR)_2(\mu_3\text{-}OR)_2]^{2+}$ core is very similar to the one found in complex **3**. The three distorted octahedral Ni^{II} atoms occupy the corners of an isosceles triangle and are separated by 3.204, 2.823 and 2.822 Å for the Ni1···Ni2, Ni2···Ni3 and Ni3···Ni1, respectively (for labelling see Fig. S1†). Two of the Ni–O distances which involve the triply bridging μ_3-O atoms [Ni3–O1 2.319(5) Å] and [Ni3–O5 2.420(5) Å] are distinguishably longer than the others which range between 1.946(6) and 2.149(5) Å.

Complex **5** crystallizes in the orthorhombic space group *Pbcn* (Table 1). Selected distances and angles are listed in Table S5.† Although complex **5** is not isostructural to **3** and **4**, it is very similar and contains two half $[Ni_3]$ molecules in the asymmetric unit (Fig. S2†). As in **3** and **4**, the Ni^{II} atoms in both $[Ni_3(\mu_2\text{-}OR)_2(\mu_3\text{-}OR)_2]^{2+}$ cores in **5** are arranged at the corners of isosceles triangles. The Ni···Ni separations are 2.849, 2.849 and 3.176 Å for the first $[Ni_3]$ and 2.844, 2.844 and 3.172 Å for the second $[Ni_3]$, respectively. The Ni–O distances and Ni–O–Ni angles are comparable within each $[Ni_3]$ triangle and compare well with those in **3** and **4**. As in **3** and **4**, two of the Ni–O distances within each $[Ni_3]$ which involve the triply bridging μ_3-O atoms are distinguishably longer (2.436 and 2.433 Å) than the others.

Magnetic properties

The variable-temperature magnetic susceptibility data for **1**, **2** and **3** were recorded between 300 and 5 K in an applied field of 1.0 kG. The magnetic data for complex **4** were the same with those of complex **3** and will not be discussed. Complex **5** with two half $[Ni_3]$ triangles within the asymmetric unit was not measured. The plots of $\chi_M T$ *versus* T for **1** and **2** are shown in Fig. 4. The $\chi_M T$ product for complex **1** increases upon cooling from a value of ~4.6 cm^3 K mol^{-1} at 300 K to a maximum value of ~10.2 cm^3 K mol^{-1} at 7 K and then slightly decreases to ~10.0 cm^3 K mol^{-1} K at 5 K. The low-temperature maximum indicates an $S = 4$ ground state and suggests the presence of dominant ferromagnetic exchange.[13] The $\chi_M T$ product for complex **2** increases upon cooling from a value of ~5.2 cm^3 K mol^{-1} at 300 K to a maximum value of ~8.9 cm^3 K mol^{-1}

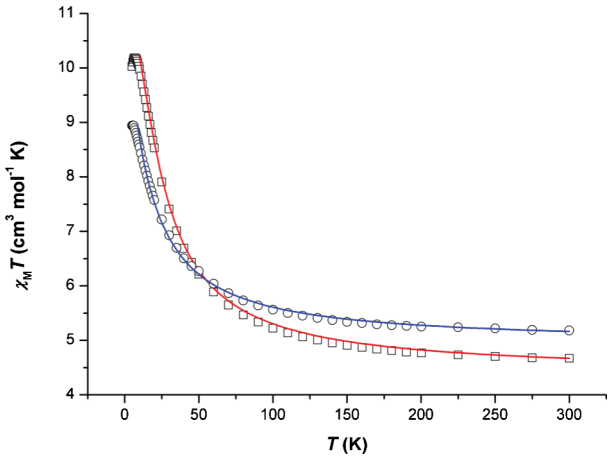

Fig. 4 $\chi_M T$ *vs.* T plots for complex **1** (□) and complex **2** (○). The solid lines represent simulation of the experimental data - see the text for details.

at 5 K. The low-temperature maximum indicates an $S = 4$ ground state, but the shape of the curve as well as the lower value of $\chi_M T$ at low temperature as compared to those of complex **1** suggest the presence of either weaker ferromagnetic interactions and/or the presence of both ferro- and antiferromagnetic interactions between the metal centers. The faint decrease in $\chi_M T$ below 7 K can be assigned to either zero-field splitting within the ground state or Zeeman effects. Considering the structural data, two exchange pathways between the metal centers are possible (Scheme 3): J_1 between the Ni^{II} atoms bridged by double R–O^- ligands [Ni1–(O,O)–Ni2#1, Ni2–(O,O)–Ni2#1 and Ni1#1–(O,O)–Ni2, Fig. 1] and J_2 between Ni1 and Ni2 which are bridged by one R–O^- and one Cl^- anion [Ni1–(O,Cl or Br)–Ni2 and Ni1#1–(O,Cl or Br)–Ni2#1]. The experimental data were satisfactorily modeled using the program MAGPACK[14] and employing the spin Hamiltonian in eqn (1) to produce the following values for complex **1**: $J_1 = +6.0$ cm^{-1}, $J_2 = +1.5$ cm^{-1} and $g = 2.09$, leading to a ground state of $S = 4$, with the first excited state ($S = 3$) located 12 cm^{-1} above the ground state.

$$\hat{H} = -2J_1\,(\hat{S}_1\cdot\hat{S}_3 + \hat{S}_2\cdot\hat{S}_3 + \hat{S}_2\cdot\hat{S}_4) - 2J_2\,(\hat{S}_1\cdot\hat{S}_2 + \hat{S}_3\cdot\hat{S}_4) \quad (1)$$

$$\hat{H} = D\hat{S}_z^{\,2} + g\mu_B\mu_0\hat{S}\cdot H \quad (2)$$

$$\hat{H} = -2J_1\,(\hat{S}_1\cdot\hat{S}_2 + \hat{S}_2\cdot\hat{S}_3) - 2J_2\,(\hat{S}_1\cdot\hat{S}_3) \quad (3)$$

The relevant values for complex **2** are: $J_1 = +6.0$ cm^{-1}, $J_2 = -1.5$ cm^{-1} and $g = 2.22$, leading to a spin ground state of $S = 4$ with the first excited state ($S = 3$) located only 2 cm^{-1} above the ground state. The value of J_1 is the same in both complexes, since the relevant Ni–O–Ni angles and Ni···Ni distances are

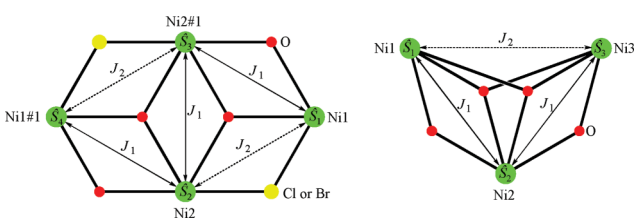

Scheme 3 Schematic detailing the 2-J models employed to simulate the experimental data for complexes **1**, **2** (left) and **3** (right).

of the same magnitude. J_2 in **2** is negative suggesting weak antiferromagnetic interactions while J_2 in complex **1** is positive suggesting weak ferromagnetic interactions. Magnetization data were collected in the ranges 0.3–5 T and 2.0–7.0 K to determine the spin ground state for both complexes. The plot of the reduced magnetization ($M/N\mu_B$) *vs* H/T for complex **1** is shown in Fig. 5. The data were fit with the aid of MAGMOFIT[14] by a matrix diagonalization method to a model that assumes only the ground state is populated, includes axial zero-field splitting (DS_z^2) and the Zeeman interaction, and carries out a full powder average. The corresponding Hamiltonian is given by eqn (2), where D is the axial anisotropy, μ_B is the Bohr magneton, μ_0 is the vacuum permeability, $\hat{S}_z$ is the easy-axis spin operator, and H is the applied field. The best fit gave $S = 4$, $D = +0.99$ cm^{-1} and $g = 2.09$. The magnetization data for complex **2** could not be satisfactorily fit with MAGMOFIT. Ac susceptibility measurements performed in the 2–10 K range in zero applied dc field and a 2.5 G ac field oscillating at 200–1000 Hz show neither in-phase nor out-of-phase signal or frequency dependence of the susceptibility.

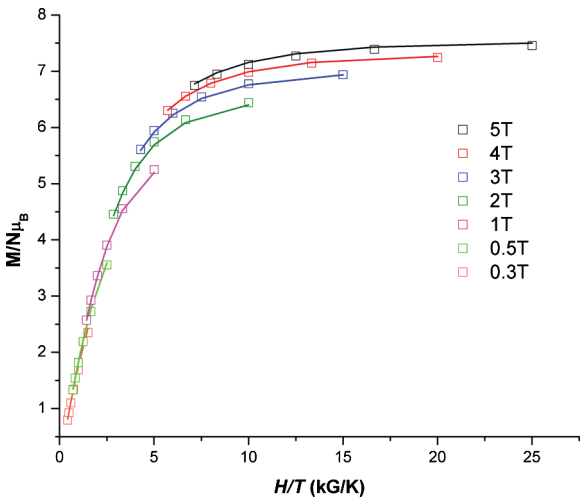

Fig. 5 Plot of reduced magnetization ($M/N\mu_B$) *versus* H/T for **1**. The solid lines correspond to the fits of the data - see text for details.

The $\chi_M T$ product of complex **3** increases upon cooling from a value of ~3.8 cm^3 K mol^{-1} at 300 K to a maximum value of ~6.5 cm^3 K mol^{-1} at 10 K and then slightly decreases to ~6.3 cm^3 K mol^{-1} K at 5 K (Fig. 6). The low-temperature maximum indicates an $S = 3$ ground state and suggests the presence of dominant ferromagnetic exchange.[13] The faint decrease in $\chi_M T$ below 10 K can be assigned to either zero-field splitting within the ground state or Zeeman effects. Inspection of the structural data reveals the presence of two exchange pathways between the Ni^{II} centres (Scheme 3): J_1 between Ni1 $\cdots$ Ni2 and Ni2 $\cdots$ Ni3, where the Ni $\cdots$ Ni distances are 2.811 and 2.815 Å, respectively, and J_2 between Ni1 and Ni3 (Ni1 $\cdots$ Ni3 = 3.187 Å). Modelling of the experimental data with the aid of MAGPACK and employing the spin Hamiltonian in eqn (2) produced the following values: $J_1 = +12.5$ cm^{-1}, $J_2 = -0.5$ cm^{-1} and $g = 2.13$, leading to a spin ground state of $S = 3$ with the first excited state ($S = 2$) located 23 cm^{-1} above the ground state. Magnetization data, collected in the ranges 0.5–5 T and 2.0–7.0 K, are plotted as the reduced magnetization ($M/N\mu_B$) *vs* H/T in Fig. 7. The experimental data were fit with the aid of MAGMOFIT

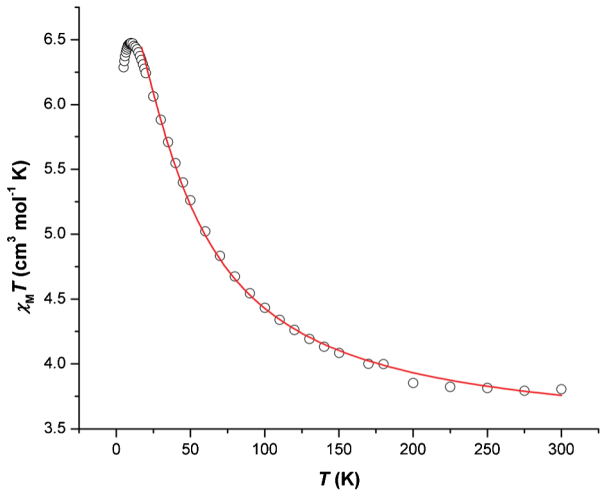

Fig. 6 $\chi_M T$ *vs.* T plot for complex **3**. The solid line represents simulation of the experimental data - see the text for details.

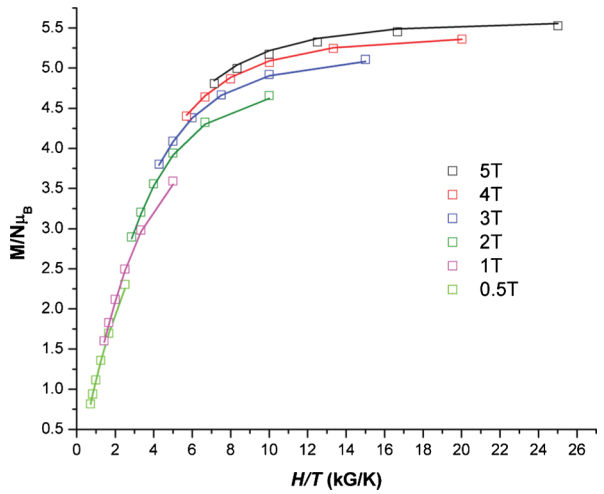

Fig. 7 Plot of reduced magnetization ($M/N\mu_B$) *versus* H/T for **3**. The solid lines correspond to the fits of the data - see text for details.

to produce the following values: $S = 3$, $D = +1.50$ cm^{-1} and $g = 2.11$. Ac susceptibility measurements performed in the 2–10 K range in zero applied dc field and a 2.5 G ac field oscillating at 250 and 1000 Hz show neither in-phase nor out-of-phase signal or frequency dependence of the susceptibility.

Discussion

The planar tetranuclear topology (also referred as defect double cubane) is widely spread in Ni^{II} chemistry. A Cambridge Structural Database[15] search reveals the presence of twenty four planar tetranuclear Ni^{II} complexes comprising the $[Ni_4L_6]^{n+}$ core (L = donor atom).[16] Eighteen of those twenty four complexes comprise the $[Ni_4(\mu_2\text{-}OR)_4(\mu_3\text{-}OR)_2]$ core, six complexes comprise the $[Ni_4(\mu_2\text{-}N_{azide})_2(\mu_2\text{-}OR)_2(\mu_3\text{-}OR)_2]$ core, one comprises the $[Ni_4(\mu_2\text{-}N_{azide})_4(\mu_3\text{-}N_{azide})_2]$ core and only one complex comprises the $[Ni_4(\mu_2\text{-}Cl)_2(\mu_2\text{-}OR)_2(\mu_3\text{-}OR)_2]$ core[17] that is similar to the one found in complex **1**. Di-2-pyridyl ketone has provided access to six[18–22] of the above mentioned twenty four Ni^{II}

Table 2 Spin ground states (S) and g for planar tetranuclear Ni^{II} complexes

Core	g	S	Ref.
$[Ni_4(\mu_2\text{-}Cl)_2(\mu_2\text{-}OR)_2(\mu_3\text{-}OR)_2]^a$	2.09	4	—
$[Ni_4(\mu_2\text{-}Br)_2(\mu_2\text{-}OR)_2(\mu_3\text{-}OR)_2]^b$	2.22	4	—
$[Ni_4(\mu_2\text{-}OR)_4(\mu_3\text{-}OR)_2]^c$	2.00	0	19
$[Ni_4(\mu_2\text{-}OR)_4(\mu_3\text{-}OR)_2]^d$	2.12	4	32
$[Ni_4(\mu_2\text{-}OR)_4(\mu_3\text{-}OR)_2]^e$	2.20	4	34
$[Ni_4(\mu_2\text{-}OR)_4(\mu_3\text{-}OR)_2]^f$	2.19	4	34
$[Ni_4(\mu_2\text{-}OR)_4(\mu_3\text{-}OR)_2]^g$	2.23	4	35
$[Ni_4(\mu_2\text{-}N_{azide})_2(\mu_2\text{-}OR)_2(\mu_3\text{-}OR)_2]^h$	2.1	4	18
$[Ni_4(\mu_2\text{-}N_{azide})_2(\mu_2\text{-}OR)_2(\mu_3\text{-}OR)_2]^i$	2.136	4	20
$[Ni_4(\mu_2\text{-}N_{azide})_2(\mu_2\text{-}OR)_2(\mu_3\text{-}OR)_2]^j$	2.1	4	21
$[Ni_4(\mu_2\text{-}N_{azide})_2(\mu_2\text{-}OR)_2(\mu_3\text{-}OR)_2]^k$	2.11	4	36
$[Ni_4(\mu_2\text{-}N_{azide})_4(\mu_3\text{-}N_{azide})_2]^l$	2.15	4	33

[a] Complex **1**. [b] Complex **2**. [c] $[Ni_4(O_2CMe)_4\{(py)_2C(OH)O\}_4]$. [d] $K_6Na_4[Ni_4(PW_9O_{34})_2(H_2O)_2]$. [e] $[Ni_4(OH)_2(H_2O)_6(ntp)_2]$. [f] $[Ni_4(OMe)_2(H_2O)_6(ntp)_2]$, H_3ntp = nitrilotripropionic acid. [g] $Na_2[H_6N_2(CH_2)_6]_2[Ni_4\{H_4N_2(CH_2)_6\}_2(H_2PW_9O_{34})_2]$. [h] $[Ni_4(N_3)_2\{py_2C(OH)O\}_2\{py_2C(OMe)O\}_2(H_2O)_2](ClO_4)_2$. [i] $[Ni_4(N_3)_4\{py_2C(OH)O\}_4]$. [j] $[Ni_4(N_3)_4\{py_2C(OH)O\}_2\{py_2C(OMe)O\}_2]$. [k] $[Ni_4(H_2L)_2(OCH_3)_2(CH_3CO_2)_2(N_3)_2]$, H_3L = 2,6-bis[(2-hydroxy-ethylimino)-methyl]-4-methylphenol. [l] $[Ni_4(N_3)_8(enbzpy)_2]$, enbzpy = *N*,*N*-bis(pyridin-2-yl)benzylidene]ethane-1,2-diamine.

Table 3 Structural and magnetic parameters for complexes $[Ni_3(L^4)_3]$, $[Ni_3(L^5)_5(HL^5)]NO_3$ and **3**[a]

	$[Ni_3(L^4)_3]$	$[Ni_3(L^5)_5(HL^5)]NO_3$	**3**
Reference	11	12	This work
g	2.14	$g_{1,2}$ = 2.183 g_3 = 2.247	2.13
S	1	3	3
J_1[b]	−2.65	+8.2	+12.5
J_2[c]	−1.35	+5.5	−1.5
Ni1 ··· Ni2	2.819	2.804	2.811
Ni1–O1–Ni2	88.21	88.74	89.50
Ni1–O3–Ni2	82.65	80.92	76.51
Ni1–O5–Ni2	81.90	81.73	79.76
Ni2 ··· Ni3	2.905	2.833	2.815
Ni2–O3–Ni3	83.22	82.31	78.04
Ni2–O5–Ni3	86.07	82.24	78.11
Ni2–O7–Ni3	92.10	89.16	89.66
Ni1 ··· Ni3	3.384	3.164	3.187
Ni1–O3–Ni3	105.40	99.48	100.54
Ni1–O5–Ni3	99.49	96.83	99.49

[a] For labelling see Fig. 3 and Scheme 3. [b] $J_1 = J_{Ni1\cdots Ni2} = J_{Ni2\cdots Ni3}$. [c] $J_2 = J_{Ni1\cdots Ni3}$.

clusters. Five more planar tetranuclear aggregates are based on Mn^{II} (1)[23] and Co^{II} (4)[23–25] and the various forms of py_2CO. The structural features of the planar tetranuclear Ni^{II} clusters which are based on the various forms of py_2CO are very similar. Among the 308 planar tetranuclear aggregates known today (of any transition metal ion),[15] only four complexes comprise the $[M_4(\mu_2\text{-}X)_2(\mu_2\text{-}OR)_2(\mu_3\text{-}OR)_2]^{n+}$ core (X = halide) found in **1** and **2**. These complexes are: $[Ni_4Cl_2(L^1)_2(HL^1)_2]$,[17] $[Cu_4(hpp)_4Cl_4]$,[26] $[Cu_4(hpp)_4Br_4]$[26] and $[Cu_4(L^2)_2(OMe)_2Cl_4]$[27] [H_2L^1 = N-(2-hydroxymethylphenyl)salicylideneimine, Hhpp = 2-(hydroxypropyl)pyridine and HL^2 = (9-methyl-2,16,5,13,18,19-dithiatetra-azatricyclo(15.2.2.17,11)docosa-1(19),5,7,9,11(22),12,17,20-octaen-22-ol].

Table 2 summarizes the planar tetranuclear Ni^{II} aggregates that have been magnetically studied. Although we can not directly compare the values of the coupling constants (J) due to the different models utilized, we can summarize the outcome of these evaluations. All complexes listed in Table 2, except one, are high spin (S = 4) as a result of the dominant ferromagnetic interactions mediated between the metal centers. Unfortunately, the only tetranuclear complex which is similar to **1** and **2**, $[Ni_4Cl_2(L^1)_2(HL^1)_2]$,[17] has not been magnetically studied. The values of J_1 (+6.0 cm^{-1} in both **1** and **2**) are equivalent in magnitude with the values obtained for other similar complexes (listed in Table 5) with Ni–O–Ni angles between ~95° and ~99.° Although, it has been documented that, in the case of mixed bridged polynuclear species, the overall exchange coupling constant cannot be ascribed on the basis of the algebraic sum of contributions coming from different bridges,[28] the value of J_2 [+1.5 cm^{-1} (**1**) and -0.5 cm^{-1} (**2**)] is in agreement with the increased Ni–O–Ni angles of 104.37° (**1**) and 106.19° (**2**) which are at the upper limit of the 90° + 14° criterion for a Ni–O–Ni angle to tolerate ferromagnetic interactions.[29] There are only two mixed bridged Ni–(O,Cl)–Ni dimers[28,30] with Ni–O–Ni and Ni–Cl–Ni angles of 103.6° (O) and 83.76° (Cl) and 105.2° (O) and 85.35° (Cl) and both exhibit weak ferromagnetic interactions. Kahn notes,[31] that, for doubly bridged Ni–X–Ni (X = Cl, Br NCS) species, J is expected to be positive when the Ni–X–Ni angles are close to 90° and negative for larger Ni–X–Ni angles. In our case, both Ni–Cl–Ni and Ni–Br–Ni angles are close to and smaller than 90° [X = Cl 88.55°(**1**) and X = Br 84.19°(**2**)].

There is only a handful of Ni^{II} triangles with a $[Ni_3(\mu_2\text{-}OR)_2(\mu_3\text{-}OR)_2]^{n+}$ core. These complexes are: $[Ni_3(mq)_6]$,[9] $[Ni_3(Hmq)(mq)_5]ClO_4$,[9] $[Ni_3(L^3)_5(MeOH)(EtOH)]Cl$,[10] $[Ni_3(L^4)_3]$[11] and $[Ni_3(L^5)_5(HL^5)]NO_3$,[12] [Hmq = 2-methyl-8-quinolinol, HL^3 = 2-(2-hydroxyphenyl)benzimidazole, H_2L^4 = *N*,*N*-bis(4,5-dimethyl-2-hydroxybenzyl)-*N*-(2-pyridylmethyl)amine, HL^5 = benzyl 2-amino-4,6-*O*-benzylidene-2-deoxy-a-d-glucopyranoside]. The first two complexes have not been magnetically studied while the third is weakly antiferromagnetically coupled. The fourth complex, $[Ni_3(L^4)_3]$,[11] is antiferromagnetically coupled with an S = 1 ground state while the fifth complex, $[Ni_3(L^5)_5(HL^5)]NO_3$,[12] is ferromagnetic with an S = 3 ground state. The last two complexes which are isosceles triangles were modelled by utilizing the same two J model (Scheme 3) that we used to model complex **3**. Table 3 summarizes the values of structural (distances and angles) and magnetic (J, S and g) parameters for the last two complexes and complex **3**. Ni1 and Ni2 as well as Ni2 and Ni3 are bridged by three R–O^- ligands with the relevant Ni–O–Ni angles spanning a range of 15.59° (from 76.51° to 92.10°), making difficult the correlation of the structural parameters (Ni–O–Ni angles) with the values of the J parameters. We do notice, though, that the acute Ni–O–Ni angles lead to higher J values. The value of the J parameter falls from +12.5 cm^{-1} for Ni–O–Ni angles between 76.51° and 89.66° to −2.65 cm^{-1} for Ni–O–Ni angles between 81.90° to 92.10°. The same conclusion can be drawn for the coupling constants between Ni1 and Ni3 which are bridged by two R–O^- ligands. The obtuse Ni–O–Ni angles lead to smaller J parameters. The value of the J parameter rises from −1.35 cm^{-1} for Ni–O–Ni angles between 99.49° and 105.40° to +5.5 cm^{-1} for Ni–O–Ni angles between 96.83° to 99.48°.

Conclusions

To conclude, the chemistry of the nickel halides (NiF_2, $NiCl_2{\cdot}6H_2O$, $NiBr_2{\cdot}6H_2O$ and $NiI_2{\cdot}6H_2O$) with di-2-pyridyl ketone resulted in two new planar tetranuclear Ni(II) clusters and three new Ni(II) triangles which are based on the hydrate and/or the hemiacetal of di-2-pyridyl ketone. The tetranuclear complexes comprise the $[Ni_4(\mu_2\text{-}X)_2(\mu_2\text{-}OR)_2(\mu_3\text{-}OR)_2]^{2+}$ (X = Cl or Br) while the presence of F^- and I^- resulted in the triangles with a $[Ni_3(\mu_2\text{-}OR)_2(\mu_3\text{-}OR)_2]^{2+}$ core. The study of magnetic properties of the tetranuclear complexes indicated that ferromagnetic interactions dominate resulting in high-spin $S = 4$ ground state. The Ni^{II} triangle is also dominated by ferromagnetic interactions which result in a high-spin $S = 3$ ground state. We are presently investigating this reaction system further by incorporating other bi- or polydentate bridging di- or poly-anionic ligands to target polymeric complexes.

Experimental

Materials and Methods

All manipulations were performed under aerobic conditions, using materials as received. IR spectra were recorded as KBr pellets in the 4000–400 cm^{-1} range on a Shimadzu FT/IR IRAffinity-1 spectrometer. Variable-temperature, solid-state direct current (dc) and alternative current (ac) magnetic susceptibility data were collected on a Quantum Design MPMS-XL SQUID magnetometer equipped with a 5 T dc magnet (University of Crete, UoC). Diamagnetic corrections were applied to the observed paramagnetic susceptibilities using Pascal's constants.

X-ray Crystallography

Data collection for compounds **1** and **3–5** was carried out at room temperature using Mo-Kα radiation (λ = 0.71073 Å) on a Bruker SMART Apex-II diffractometer. Low temperature data for compound **2** were collected on an Excalibur Cappa CCD instrument. The crystals were sealed in glass capillaries to minimize destruction caused by the release of clathrate solvents. The structures were solved by direct methods. The coordinates of nickel atoms were extracted from the initial solutions and the other non-hydrogen atoms were located then in difference Fourier syntheses. All non-hydrogen atoms were refined by full-matrix techniques first in isotropic and then, where possible, in anisotropic approximation. Hydrogen atoms coordinates were calculated geometrically and included into the final refinement in isotropic approximation. The details of data collection and refinement can be found in Table 1. The specific difficulties encountered in the structure studies of **1**–**5** are discussed here below.

Compound 1. The clathrate nature of the product was in this case not hindering data collection. Only solvent non-hydrogen atoms were left isotropic in the final refinement. The clathrate ether molecule is disordered between at least two positions, of which the principal one defined by the oxygen atom O(50) was fully identified, while the other, defined by O(50A) could be resolved only partially in the view of low residual electron density.

Compound 2. The clathrate nature of the product required low temperature data collection. Bigger voids for solvent imposed by the bigger anion size resulted also in more pronounced thermal disorder for the clathrate ether molecules. Only solvent non-hydrogen atoms were left isotropic in the final refinement.

Compound 3. The peculiar disorder, resulting from partial occupation of a void by iodide ion and by a methanol molecule could be successfully resolved, but the non-hydrogen atoms in the clathrate alcohol molecules were left isotropic. It should be mentioned that the disorder of the iodide anions is practically continuous in the void and the model introducing defined positions describes it with only limited resolution as indicated by their elongated thermal ellipsoids.

Compound 4. The structure contained considerable empty voids that did not contain any residual electron density. Non-hydrogen atoms in the located clathrate solvent molecules were left in isotropic approximation. The peculiar disorder between the iodide and nitrate anion in this structure could be partially resolved, revealing even possibility for different orientations of the nitrate ion in the huge empty voids present in this structure.

Compound 5. The disorder between the fluoride and hexafluorosilicate anions and between the partially occupied positions within the hexafluoride anion could be resolved successfully. The anions $[SiF_6]^{2-}$ and F^- are situated in general positions and their occupations were estimated from the corresponding electron densities and refined as fixed values 0.8 for $[SiF_6]^{2-}$, producing the charge of −1.6, and −0.4 for the fluoride F(1), which gives the sum of negative charges −2, correlating with the positive charge +2 of the $[Ni_3(\mu_2\text{-}OR)_2(\mu_3\text{-}OR)_2]^{2+}$ cations. Packing effects in this structure are apparently dominating over the possible charge interactions, so that no "fluoride" bonding to other non-hydrogen atoms in the structure could be revealed. The non-hydrogen atoms within the clathrate alcohol molecules were left in isotropic approximation.

Synthesis

$[Ni_4Cl_2\{py_2C(OH)O\}_2\{py_2C(OMe)O\}_2(MeOH)_2]Cl_2{\cdot}2Et_2O$ (1·2Et$_2$O). $NiCl_2{\cdot}6H_2O$ (0.030 g, 0.125 mmol) and $(py)_2CO$ (0.023 g, 0.125 mmol) were dissolved in methanol (10 mL) to produce a clear pale green solution. Et_3N (0.018 mL, 0.125 mmol) was then added and the solution darkens. X-ray quality green crystals of **1**·2Et$_2$O were formed over a period of a week after Et_2O (20 mL) diffusion. The crystals were collected by vacuum filtration, washed with methanol (3 mL) and Et_2O (2 × 5 mL) and dried in air. Yield: 0.031 g, 77%. Elemental analysis (%) calcd for **1** $C_{48}H_{48}N_8O_{10}Cl_4Ni_4$: C 45.27, H 3.80, N 8.80, found: C 45.33, H 3.85, N 8.90.

$[Ni_4Br_2\{py_2C(OH)O\}_2\{py_2C(OMe)O\}_2(MeOH)_2]Br_2{\cdot}2Et_2O$ (2·2Et$_2$O). $NiBr_2{\cdot}3H_2O$ (0.170 g, 0.624 mmol) and $(py)_2CO$ (0.115 g, 0.624 mmol) were dissolved in methanol (15 mL) to produce a clear pale green solution. Et_3N (0.089 mL, 0.624 mmol) was then added and the solution darkens. X-ray quality green crystals of **2**·2Et$_2$O were formed over a period of two weeks after Et_2O (30 mL) diffusion. The crystals were collected by vacuum filtration, washed with methanol (3 mL) and Et_2O (2 × 5 mL) and dried in air. Yield: 0.118 g, 52%. Elemental analysis (%) calcd for **2** $C_{48}H_{48}N_8O_{10}Br_4Ni_4$: C 39.72, H 3.33, N 7.72, found: C 39.80, H 3.40, N 7.80.

$[Ni_3\{py_2C(OMe)O\}_4]I_2\cdot 2.6MeOH$ (3·2.6MeOH). $NiI_2\cdot 6H_2O$ (0.200 g, 0.475 mmol) and $(py)_2CO$ (0.087 g, 0.475 mmol) were dissolved in methanol (15 mL) to produce a clear pale green solution. Et_3N (0.067 mL, 0.475 mmol) was then added and the solution slightly darkens. X-ray quality green crystals of **3**·2MeOH were formed over a period of two weeks with Et_2O (30 mL) diffusion. The crystals were collected by vacuum filtration, washed with methanol (3 mL) and Et_2O (2 × 5 mL) and dried in air. Yield: 0.098 g, 47%. Elemental analysis (%) calcd for **3** $C_{48}H_{44}N_8O_8I_2Ni_3$: C 44.66, H 3.44, N 8.68, found: C 44.53, H 3.71, N 8.51.

$[Ni_3\{py_2C(OMe)O\}_4](NO_3)_{0.65}I_{1.35}\cdot 2MeOH$ (4·2MeOH). $Ni(NO_3)_2\cdot 6H_2O$ (0.138 g, 0.475 mmol), NaI (0.710 g, 4.74 mmol) and $(py)_2CO$ (0.087 g, 0.475 mmol) were dissolved in methanol (15 mL) to produce a clear pale green solution. Et_3N (0.067 mL, 0.475 mmol) was then added and the solution slightly darkens. X-ray quality green crystals of **4**·2MeOH were formed over a period of two weeks after Et_2O (30 mL) diffusion. The crystals were collected by vacuum filtration, washed with methanol (2 × 3 mL) and Et_2O (2 × 5 mL) and dried in air. Yield: 0.08 g, 40%. Elemental analysis (%) calcd for **4** $C_{48}H_{44}N_{8.65}O_{9.95}I_{1.35}Ni_3$: C 46.17, H 3.55, N 9.70, found: C 45.67, H 3.71, N 9.51.

$[Ni_3\{py_2C(OMe)O\}_4](SiF_6)_{0.8}F_{0.4}\cdot 3.5MeOH$ (5·3.5MeOH). A methanolic solution (15 ml) of NiF_2 (0.100 g, 1.035 mmol) and $(py)_2CO$ (0.189 g, 1.035 mmol) was heated under reflux for 1 h to produce a clear green solution. The resulting solution was cooled to room temperature and Et_3N (0.146 mL, 1.035 mmol) was added to produce a clear blue-green solution. X-ray quality green crystals of **5**·2.5MeOH were formed over a period of four to six weeks after Et_2O (30 mL) diffusion. The crystals were collected by vacuum filtration, washed with methanol (3 mL) and Et_2O (2 × 5 mL) and dried in air. Yield: 0.06 g, 15%. Elemental analysis (%) calcd for $C_{48}H_{44}N_8O_8F_{5.2}Si_{0.8}Ni_3$: C 49.77, H 3.83, N 9.67, found: C 49.75, H 3.73, N 9.71.

Acknowledgements

G.S.P. is grateful to the Special Account for Research Grants (SARG) of the National and Kapodistrian University of Athens for partial support of this work. The authors express their sincerest gratitude to Dr Daniel Avignant at the University of Clermont-Ferrand, France, for the assistance with data collection for complex **2** at room temperature and to Dr Lars Eriksson at Stockholm University for the low temperature data collection for the same compound. The support from the Swedish Research Council (Vetenskapsrådet) is gratefully acknowledged.

Notes and references

1 R. E. P. Winpenny, in *Comprehensive Coordination Chemistry II* (ed., J. A. McCleverty and T. J. Meyer), Elsevier, Amsterdam, 2004, vol. 7, ch. 7.3, pp. 125–175; E. K. Brechin, *Chem. Commun.*, 2005, 5141; A. J. Tasiopoulos and S. P. Perlepes, *Dalton Trans.*, 2008, 5537; A. M. Ako, I. J. Hewitt, V. Mereacre, R. Clerac, W. Wernsdorfer, C. E. Anson and A. K. Powell, *Angew. Chem., Int. Ed.*, 2006, **45**, 4926.
2 E. Cremades, J. Cano, E. Ruiz, G. Rajaraman, C. J. Milios and E. K. Brechin, *Inorg. Chem.*, 2009, **48**, 8012; R. Inglis, L. F. Jones, C. J. Milios, S. Datta, A. Collins, S. Parsons, W. Wernsdorfer, S. Hill, S. P. Perlepes, S. Piligkos and E. K. Brechin, *Dalton Trans.*, 2009, 3403; C. J. Milios, R. Inglis, A. Vinslava, R. Bagai, W. Wernsdorfer, S. Parsons, S. P. Perlepes, G. Christou and E. K. Brechin, *J. Am. Chem. Soc.*, 2007, **129**, 12505; R. Inglis, S. M. Taylor, L. F. Jones, G. S. Papaefstathiou, S. P. Perlepes, S. Datta, S. Hill, W. Wernsdorfer and E. K. Brechin, *Dalton Trans.*, 2009, 9157.
3 D. J. Tranchemontagne, J. L. Mendoza-Cortes, M. O'Keeffe and O. M. Yaghi, *Chem. Soc. Rev.*, 2009, **38**, 1257 and references cited therein.
4 Y.-L. Bai, J. Tao, R.-B. Huang and L.-S. Zheng, *Angew. Chem., Int. Ed.*, 2008, **47**, 5344; G. A. Timco, E. J. L. McInnes, R. G. Pritchard, F. Tuna and R. E. P. Winpenny, *Angew. Chem., Int. Ed.*, 2008, **47**, 9681; J. Choi, J. Park, M. Park, D. Moon and M. S. Lah, *Eur. J. Inorg. Chem.*, 2008, 5465.
5 J. J. Perry IV, J. A. Perman and M. J. Zaworotko, *Chem. Soc. Rev.*, 2009, **38**, 1400 and references cited therein.; Y. Liu, J. F. Eubank, A. J. Cairns, J. Eckert, V. C. Kravtsov, R. Luebke and M. Eddaoudi, *Angew. Chem., Int. Ed.*, 2007, **46**, 3278; Z. Zheng and X. Tu, *CrystEngComm*, 2009, **11**, 707; F. Nouar, J. F. Eubank, T. Bousquet, L. Wojtas, M. J. Zaworotko and M. Eddaoudi, *J. Am. Chem. Soc.*, 2008, **130**, 1833; S. Hu and M.-L. Tong, *Dalton Trans.*, 2005, 1165.
6 C. C. Stoumpos, R. Inglis, G. Karotsis, L. F. Jones, A. Collins, S. Parsons, C. J. Milios, G. S. Papaefstathiou and E K. Brechin, *Cryst. Growth Des.*, 2009, **9**, 24; R. Inglis, A. D. Katsenis, A. Collins, F. White, C. J. Milios, G. S. Papaefstathiou and E. K. Brechin, *CrystEngComm*, 2010, **12**, 2064.
7 A. D. Katsenis, R. Inglis, A. M. Z. Slawin, V. G. Kessler, E. K. Brechin and G. S. Papaefstathiou, *CrystEngComm*, 2009, **11**, 2117.
8 G. S. Papaefstathiou and S. P. Perlepes, *Comments Inorg. Chem.*, 2002, **23**, 249.
9 A. Yuchi, H. Murakami, M. Shiro, H. Wada and G. Nakagawa, *Bull. Chem. Soc. Jpn.*, 1992, **65**, 3362.
10 X. Yun, J. Min, L. Jun, W. Chen, Y. Jun-Feng and Z. Feng-Xing, *Acta Chim. Sinica*, 2006, **64**, 1183.
11 E. Labisbal, L. Rodrıguez, O. Souto, A. Sousa-Pedrares, J. A. Garcıa-Vazquez, J. Romero, A. Sousa, M. Yanez, F. Orallo and J. A. Real, *Dalton Trans.*, 2009, 8644.
12 A. Burkhardt, E. T. Spielberg, S. Simon, H. Gorls, A. Buchholz and W. Plass, *Chem.–Eur. J.*, 2009, **15**, 1261.
13 C. J. Milios, A. Prescimone, J. Sanchez-Benitez, S. Parsons, M. Murrie and E. K. Brechin, *Inorg. Chem.*, 2006, **45**, 7053.
14 MAGPACK: J. J. Borras-Almenar, J. M. Clemente-Juan, E. Coronado and B. S. Tsukerblat, *Inorg. Chem.*, 1999, **38**, 6081; J. J. Borrás-Almenar, J. M. Clemente-Juan, E. Coronado and B. S. Tsukerblat, *J. Comput. Chem.*, 2001, **22**, 985. MAGMOFIT: Stergios Piligos, University of Copenhagen.
15 F. H. Allen, *Acta Crystallogr., Sect. B: Struct. Sci.*, 2002, **58**, 380.
16 A list with the 24 refcodes is provided in Table S6 (ESI†).
17 M. Koikawa, M. Ohba and T. Tokii, *Polyhedron*, 2005, **24**, 2257.
18 Z. E. Serna, L. Lezama, M. K. Urtiaga, M. I. Arriortua, M. G. Barandika, R. Cortes and T. Rojo, *Angew. Chem., Int. Ed.*, 2000, **39**, 344.
19 C. G. Efthymiou, C. P. Raptopoulou, A. Terzis, R Boca, M. Korabic, J. Mrozinski, S. P. Perlepes and E. G. Bakalbassis, *Eur. J. Inorg. Chem.*, 2006, 2236.
20 Z. E. Serna, M. G. Barandika, R. Cortes, M. K. Urtiaga, G. E. Barberis and T. Rojo, *J. Chem. Soc., Dalton Trans.*, 2000, 29.
21 D.-Y. Wu, W. Huang, W.-J. Hua, Y. Song, C.-Y. Duan, S.-H. Li and Q.-J. Meng, *Dalton Trans.*, 2007, 1838.
22 S. B. Jedner, H. Schwoppe, H. Nimir, A. Rompel, D. A. Brown and B. Krebs, *Inorg. Chim. Acta*, 2002, **340**, 181.
23 G. S. Papaefstathiou, A. Escuer, C. P. Raptopoulou, A. Terzis, S. P. Perlepes and R. Vicente, *Eur. J. Inorg. Chem.*, 2001, 1567.
24 M. G. Barandika, Z. Serna, R. Cortes, L. Lezama, M. K. Urtiaga, M. I. Arriortua and T. Rojo, *Chem. Commun.*, 2001, 45; Z. E. Serna, M. K. Urtiaga, M. G. Barandika, R. Cortes, S. Martin, L. Lezama, M. I. Arriortua and T. Rojo, *Inorg. Chem.*, 2001, **40**, 4550.
25 G. S. Papaefstathiou, A. Escuer, M. Font-Bardia, S. P. Perlepes, X. Solans and R. Vicente, *Polyhedron*, 2002, **21**, 2027.
26 N. Lah, I. Leban and R. Clerac, *Eur. J. Inorg. Chem.*, 2006, 4888.
27 S. S. Tandon, L. K. Thompson, J. N. Bridson and M. Bubenik, *Inorg. Chem.*, 1993, **32**, 4621.
28 A. Banerjee, R. Singh, D. Chopra, E. Colacio and K. Krishna Rajak, *Dalton Trans.*, 2008, 6539.

29 J. A. Bertrand, A. P. Ginsberg, R. I. Kaplan, C. E. Kirkwood, R. L. Martin and R. C. Sherwood, *Inorg. Chem.*, 1971, **10**, 240.
30 E. R. Quijano, E. D. Stevens and C. J. O'Connor, *Inorg. Chim. Acta*, 1990, **177**, 267.
31 O. Kahn, *Molecular Magnetism*, VCH, New York, 1993.
32 J. M. Clemente-Juan, E. Coronado, J. R. Galan-Mascaros and C. J. Gomez-Garcıa, *Inorg. Chem.*, 1999, **38**, 55.
33 T. K. Karmakar, S. K. Chandra, J. Ribas, G. Mostafa, T. H. Luc and B. K. Ghosh, *Chem. Commun.*, 2002, 2346.
34 P. King, R. Clerac, W. Wernsdorfer, C. E. Anson and A. K. Powell, *Dalton Trans.*, 2004, 2670.
35 Z. Zhang, J. Liu, E. Wang, C. Qin, Y. Li, Y. Qi and X. Wang, *Dalton Trans.*, 2008, 463.
36 S. S. Tandon, S. D. Bunge, R. Rakosi, Z. Xu and L. K. Thompson, *Dalton Trans.*, 2009, 6536.

